Environmental Science
Processes & Impacts

PAPER

Cite this: *Environ. Sci.: Processes Impacts*, 2014, **16**, 2127

Chromium(III) oxidation by biogenic manganese oxides with varying structural ripening†

Yuanzhi Tang,*[a] Samuel M. Webb,[b] Emily R. Estes[c] and Colleen M. Hansel*[c]

Received 7th February 2014
Accepted 27th June 2014

DOI: 10.1039/c4em00077c

rsc.li/process-impacts

Manganese (Mn) oxides, which are generally considered biogenic in origin within natural systems, are the only oxidants of Cr(III) under typical environmental conditions. Yet the influence of Mn biooxide mineral structural evolution on Cr(III) oxidation under varying geochemical conditions is unknown. In this study we examined the role of light, organic carbon, pH, and the structure of biogenic Mn oxides on Cr(III) oxidation. Aging of Mn oxides produced by a marine bacterium within the widespread *Roseobacter* clade resulted in structural ripening from a colloidal hexagonal to a particulate triclinic birnessite phase. The structurally diverse Mn oxides were then reacted with aqueous Cr(III) within artificial seawater in the presence or absence of carbon and light. Here we found that Cr(III) oxidation capacity was highest at near neutral pH and in the combined presence of carbon and light. Mn oxide ripening from a hexagonal to a triclinic birnessite phase led to decreased Cr(III) oxidation in the presence of carbon and light, whereas no change in reactivity was observed in the absence of carbon and/or in the dark. As only minimal Cr(III) oxidation was observed in the absence of Mn oxides, these results strongly point to coupled Mn oxide- and photo-induced generation of organic and/or oxygen radicals involved in Cr(III) oxidation. Based on Mn oxide concentration and structural trends, we postulate that Mn(II) produced from the oxidation of Cr(III) by the primary Mn oxide is recycled in the presence of organics and light conditions, (re)generating secondary hexagonal birnessite and thereby allowing for continuous oxidation of Cr(III). In the absence of this Mn oxide regeneration, Cr(III) induced structural ripening of the hexagonal birnessite precludes further Cr(III) oxidation. These results highlight the complexity of reactions involved in Mn oxide mediated Cr(III) oxidation and suggest that photochemical carbon reactions are requisite for sustained Cr(III) oxidation and persistence of reactive Mn oxides.

Environmental impact

Chromium (Cr) is a widespread anthropogenic contaminant in the ecosystem and human health. Transformation of the micronutrient and less mobile species Cr(III) to highly mobile and toxic Cr(VI) is strongly mediated by manganese (Mn) oxides. In fact, Mn oxides are the only oxidants of Cr(III) under most environmental conditions. Although Mn oxides are generally considered biogenic in origin, few studies have addressed the coupled role of reaction conditions and the biogenic Mn oxide structure in Cr(III) oxidation. In this study we examined the effect of light, organic carbon content, pH, and structural ripening of biogenic manganese oxides on Cr(III) oxidation using Mn oxides produced by a marine bacterium within the widespread *Roseobacter* clade.

1. Introduction

Chromium (Cr) is a significant anthropogenic metal contaminant in soils and aquatic systems due to its widespread industrial applications. The toxicity and transport behavior of Cr depend strongly on its valence state, with hexavalent and trivalent being the most common oxidation states. Cr(VI) compounds are typically soluble, mobile, and bioaccessible, and are considered carcinogenic upon inhalation exposure. Cr(III) generally forms insoluble (oxyhydr)oxides and is an essential micronutrient.[1,2]

In terrestrial and aquatic systems, a variety of compounds are capable of reducing Cr(VI) to Cr(III), such as organic matter, Fe(II), and reduced sulfur species.[1,3–5] Following reduction, Cr(III) precipitates as pure Cr(III) or mixed Cr(III)–Fe(III) (oxy)hydroxide phases that have low solubility and typically lack long range structural order.[6,7] However, under common environmental conditions, Mn(III,IV) (oxyhydr)oxides (hereafter referred to as Mn oxides) are capable of oxidizing Cr(III) to Cr(VI) and are, in fact, considered the only environmentally relevant Cr(III)

[a]*School of Earth and Atmospheric Sciences, Georgia Institute of Technology, 311 Ferst Dr, Atlanta, GA 30332-0340, USA. E-mail: yuanzhi.tang@eas.gatech.edu; Tel: +1-404-894-3814*

[b]*Stanford Synchrotron Radiation Lightsource, Menlo Park, CA 94025, USA*

[c]*Marine Chemistry and Geochemistry Department, Woods Hole Oceanographic Institution, Woods Hole, MA 02543, USA. E-mail: chansel@whoi.edu; Tel: +1-508-289-3738*

† Electronic supplementary information (ESI) available: XANES of reference compounds, unreacted, and reacted Mn oxides; Mn K-edge EXAFS fitting results of reference compounds and bioMnOx before and after reaction with Cr(III); Cr oxidation capacity as a function of bioMnOx concentration. See DOI: 10.1039/c4em00077c

oxidant.[5,8,9] Given the widespread presence of Mn oxides within the environment, understanding reaction conditions and mechanisms of Mn oxide mediated Cr(III) oxidation is important for predicting Cr mobility and transport. Several previous studies have investigated the kinetics and mechanisms of Cr(III) oxidation by abiotic (synthetic or natural) Mn oxides, such as δ-MnO_2,[3,10–12] birnessite,[11–17] manganite,[18] todorokite,[15] pyrolusite,[5] and hydrous manganese oxide.[19] It has been generally found that the rate and extent of Cr(III) oxidation were affected by the type and structure of Mn oxides.[15,20–22] In particular, Mn oxides with hexagonal symmetry (biogenic Mn oxide and birnessite) have shown the highest oxidation capacity for Cr(III).[22]

Natural Mn oxides are believed to form primarily by Mn(II) oxidation *via* either direct or indirect microbial activity.[23] The predominant type of biogenic Mn oxide formed at circumneutral pH is a highly disordered, nanocrystalline, phyllomanganate phase, similar to hexagonal birnessite.[24–26] This phase is highly reactive and can undergo abiotic transformation and ripening to form more ordered and crystalline phases such as todorokite, feitknechtite, and triclinic birnessite.[24,27–29] Due to their greater disorder and surface area, biogenic oxides are considered more reactive than their synthetic analogs.[24,25,30] Yet, only a few studies have examined Cr(III) oxidation by Mn oxides produced by microorganisms, such as the Mn(II)-oxidizing bacteria *Pseudomonas putida*[22,31–33] and *Bacillus* sp.[22,32] These studies either used the fresh biogenic Mn oxides (with a layered structure similar to δ-MnO_2) or characterized the coupled Mn(II)–Cr(III) oxidation in the presence of active microbial Mn(II)-oxidizing activity. To the best of our knowledge, no previous studies have examined the impact of natural structural transformations of biogenic Mn oxides on their reactivity toward Cr(III) oxidation.

Microorganisms (both bacteria and fungi) that are capable of oxidizing Mn(II) to Mn(III,IV) oxides are widespread in both marine and terrestrial settings, as well as contaminated sites.[23,34,35] Recently, Mn(II) oxidation by some bacterial and fungal species has been linked to the extracellular production of the reactive oxygen species (ROS) superoxide.[34–36] Oxidation by a bacterium (*Roseobacter* sp. AzwK-3b) within the widespread and abundant *Roseobacter* clade was attributed to an exoprotein (extracellular), such that superoxide production and Mn(II) oxidation activity occurred outside the cell and thus activity was maintained in cell-free filtrate.[36,37] The initial oxidation of Mn(II) by these exoproteins within the cell-free filtrate results in the formation of a highly reactive colloidal birnessite phase with hexagonal symmetry and similar in structure to δ-MnO_2. This initial hexagonal birnessite phase is highly reactive and induces the secondary abiotic oxidation of Mn(II). Mn(II)-induced aging of this colloidal phase introduces structural reorganization and the gradual transformation to a particulate phase with trigonal symmetry and minimal reactivity toward aqueous Mn(II).[27] Abiotic oxidation of Mn(II) at the colloidal hexagonal birnessite surface was substantially enhanced in the presence of light and organic carbon and diminished in the presence of superoxide scavengers (*e.g.*, superoxide dismutase – SOD), indicating a role for ROS and organic radicals in Mn(II) oxidation. Further, it illustrates a tight coupling between microbial and mineral surface chemical processes responsible for the oxidation of Mn(II). Given the structural evolution and subsequent changes in reactivity of biogenic Mn oxides, this system provides an ideal opportunity for studying the structure–reactivity relationship of biogenic Mn oxides in the oxidation of Cr(III).

Accordingly, in this study, we examined the oxidation of Cr(III) by Mn oxides produced by biogenic extracellular superoxide over the course of mineral structural evolution. We further explored the impact of pH, organic carbon content, and light on Cr(III) oxidation by these structurally diverse biogenic oxides. Given the widespread presence of Mn(II) oxidizing microorganisms in the environment, results from this study provide important insights regarding the reactivity of biogenic Mn oxides, as well as the fundamental basis for predicting and understanding Cr fate and transport behavior in nature.

2. Materials and methods

2.1. Bacterial growth and biogenic Mn oxide harvesting process

Roseobacter sp. AzwK-3b was grown in an organic carbon rich (K) medium containing 2 g L^{-1} peptone, 0.5 g L^{-1} yeast extract, and 20 mM HEPES buffer prepared with 75 vol% artificial seawater (ASW), pH 7.2 at 25 °C and 150 rpm (ref. 37) without $MnCl_2$. The ASW contains 0.3 mol L^{-1} NaCl, 0.05 mol L^{-1} $MgSO_4$, 0.01 mol L^{-1} $CaCl_2$, and 0.01 mol L^{-1} KCl. After growing *R.* AzwK-3b to the mid-exponential phase (OD_{600} ∼ 0.12), cell free filtrate was collected by centrifuging the growth culture at 8000 rpm for 10 min and passing the supernatant through a 0.45 μm filter. The resulting solution is hereafter referred to as a cell free filtrate, which maintains the activity for extracellular enzymatic superoxide production[27,36] and is used for producing biogenic Mn oxides.

Biogenic Mn oxides (hereinafter referred to as bioMnOx) were produced by reacting the cell free filtrate with 100 μM $MnCl_2$ at 25 °C and 150 rpm in the presence of ambient light. BioMnOx were aged and harvested at various time points (4–211 h) by centrifuging at 9000 rpm for 25 min and washing with deionized water (18 MΩ cm).

2.2. Cr(III) oxidation experiments

Harvested bioMnOx were resuspended in 50 mL of sterile K medium or ASW at pH 6.2 or 7.2 (buffered by 20 mM HEPES) and tested for Cr(III)-oxidizing capacity in the presence or absence of light. The initial bioMnOx concentration was ∼40 μM, measured as the Mn(III,IV) oxide concentration using the Leucoberlelin blue (LBB) method (see details below).[38] Cr(III) was added as $CrCl_3$ from a 100 mM sterile stock solution to achieve an initial concentration of 50 μM. Flasks containing the suspension were shaken at 25 °C and 150 rpm for ∼200 h in the absence (dark condition) or presence of ambient light (light condition). For experiments conducted under dark conditions, all solutions were prepared in bottles wrapped with aluminum foil, and the reaction flasks were further covered with a cardboard box. Sampling was done without direct light exposure. Control experiments were conducted at the same Cr(III)

concentration and reaction conditions without the addition of bioMnOx. The effect of bioMnOx concentration on the Cr(III) oxidation was also explored using up to 4 times concentrated bioMnOx (*i.e.*, 1× to 4× of 40 μM Mn(III,IV) oxide) and an initial Cr(III) concentration of 50 μM. All experiments were conducted in duplicate.

During the course of reaction, Mn oxide loss and Cr(VI) production were constantly monitored. Concentrations of Mn(III,IV) oxides were quantified using the Leucoberlelin blue (LBB) method with a UV-Vis spectrophotometer (Cary 50, Varian).[38] Standard curves were obtained using LBB and synthetic δ-MnO_2.[25] The concentration of Cr(VI) in the reacting suspension was analyzed using the *s*-diphenyl carbazide method.[9] To account for unavoidable minor variations in initial Mn oxide content, a Cr oxidation capacity is used to normalize the amount of Cr(VI) production to the initial Mn(III,IV) oxide concentration, defined as:

$$\text{Cr oxidation capacity} = [\text{Cr(VI)}]/[\text{Mn(III,IV) oxide}]_{\text{ini}},$$

2.3. X-ray absorption spectroscopy analysis

X-ray absorption spectroscopy (XAS) data were collected on the bioMnOx before and after reaction with Cr(III) to identify speciation and structural changes. Suspensions containing Mn oxides were vacuum filtered through 0.2 μm polycarbonate membranes and rinsed with DI water. The moist filter membranes loaded with Mn oxide wet pastes were then mounted in a Teflon sample holder covered with Kapton tape for XAS data analysis. Samples were frozen at −20 °C and thawed prior to analysis. Manganese K-edge XAS spectra were collected at beamline 11-2 at Stanford Synchrotron Radiation Lightsource (SSRL) and beamline X18B at National Synchrotron Light Source, Brookhaven National Laboratory (NSLS-BNL) with a Si (220) or (111) double crystal monochromator (40% detuning), respectively. Energy calibration was achieved using Mn foil (6539 eV). Data were collected in both fluorescence and transmission mode using a 30-element Ge solid-state detector with a Cr filter at beam line 11-2 (SSRL) or a PIPS detector at beam line X18B (NSLS). Analysis of the near edge region of consecutive XAS spectra for each sample showed no photo-induced reduction of Mn oxides under the X-ray beam.

Analysis of the bulk XAS data was performed using the programs SIXPACK[39] and Ifeffit.[40] The composition and structure of Mn oxides were determined using both the XANES (X-ray absorption near edge structure) and EXAFS (extended X-ray absorption fine structure) regions. For EXAFS analysis, spectra were background-subtracted, k^3-weighted and analyzed from 3–12 $Å^{-1}$. As previously described,[24,27] principal component analysis (PCA), combined with target transformation and linear combination fitting (LCF), was performed on the EXAFS spectra to establish the number of components representing the entire dataset. A spectral reference library of model Mn compounds was used to identify and quantify the structural components. The model compounds used were previously described,[24] and include: δ-MnO_2, triclinic Na-birnessite, hexagonal Ca-birnessite, groutite (α-MnOOH), feitknechtite (β-MnOOH), manganite (γ-MnOOH), hausmannite (Mn_3O_4), synthetic todorokite [(Na,Ca,K)(Mg,Mn)$Mn_6O_{14}\cdot 5H_2O$], pyrolusite (β-MnO_2), synthetic Mn_2O_3, aqueous Mn(III) pyrophosphate, aqueous $MnCl_2$, and aqueous $MnSO_4$.

To determine the detailed structure of the nanoparticulate and highly disordered manganese oxides, a full multiple scattering model[26] that is sensitive to the bending of the Mn octahedral layer and Mn site vacancies was used to conduct shell-by-shell EXAFS fitting. This model has been previously described in detail[26,27] and is briefly summarized below. The model consists of all single scattering (SS) paths and three types of collinear multiple scattering (MS) paths. The amplitude of all MS paths is strongly affected by the level of distortion of the phyllomanganate layers, which is accounted for as an out-of-plane bending angle β (along the *a*-axis).[26,41] A parameter f_{occ} characterizes the lattice occupancy and accounts for both the vacancies within the phyllomanganate layer as well as edge effects in nanoparticulate Mn oxides.

3. Results and discussion

3.1. Production of structurally evolved Mn oxides

Similar to previous observations,[24–26] the predominant form of biogenic Mn oxides formed at circumneutral pH was a highly disordered layered phyllomanganate phase with hexagonal symmetry. Principle component analysis (PCA) using a suite of Mn reference compounds indicated that two components were needed to reconstruct all of the unreacted bioMnOx Mn EXAFS spectra, and these components were identified as a hexagonal birnessite phase (δ-MnO_2) and a triclinic birnessite phase (Na-birnessite) (Fig. 1a). The difference between these two structures are most distinctive at around 7–10 $Å^{-1}$ in *k* space (gray shading in Fig. 1a). The hexagonal phase shows two distinct peaks at ~8 and 9 $Å^{-1}$, whereas for the triclinic phase the 8 $Å^{-1}$ oscillation decreases in amplitude accompanied by a broadening of the feature at ~9 $Å^{-1}$. Linear combination fitting (LCF) using the two reference compounds yielded good fits for all bioMnOx samples (Table S1† and Fig. 1b dotted line). The structure of the fresh (4 h) bioMnOx was composed of 100% hexagonal birnessite, and appeared as brownish suspended colloids. Upon aging, a triclinic birnessite structure was needed to fit the bioMnOx spectra. With increased aging time, the fraction of the triclinic birnessite phase increased, and the bioMnOx also aggregated to larger dark brown to black particles. At 211 h, the bioMnOx structure was best fit with 56% hexagonal and 44% triclinic birnessite. A near linear relationship ($R^2 = 0.9238$) between the fraction of hexagonal birnessite phase and aging time was observed (Fig. 1b), suggesting a strong correlation between bioMnOx structure and aging time.

These results are consistent with previous experiments using the same organism and similar experimental conditions.[27] In detail, Learman *et al.*[27] reported the transformation of bioMnOx from a pure hexagonal birnessite phase at 4 h to a 45% hexagonal/55% triclinic phase at 96 h. Similarly, using synchrotron X-ray diffraction and absorption spectroscopy, Webb *et al.*[26] found that the initial bioMnOx produced by the spores of a

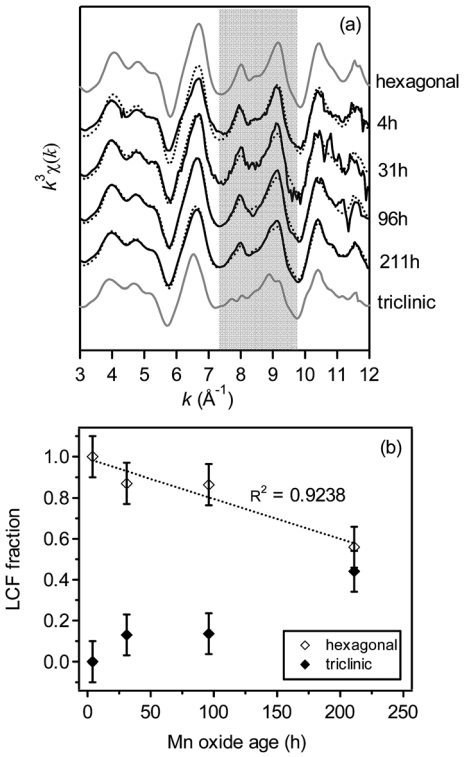

Fig. 1 (a) Linear combination fitting (LCF) results of unreacted bio-MnOx at different ages, with raw and fitted data in solid and dotted black lines, respectively. Also shown are the two end member spectra (gray lines) used for LCF, a hexagonal birnessite (δ-MnO_2) and triclinic Na-birnessite. (b) Corresponding LCF fraction of hexagonal and triclinic birnessite for the bioMnOx. Dotted line is a linear fitting of the hexagonal data (R^2 = 0.9238).

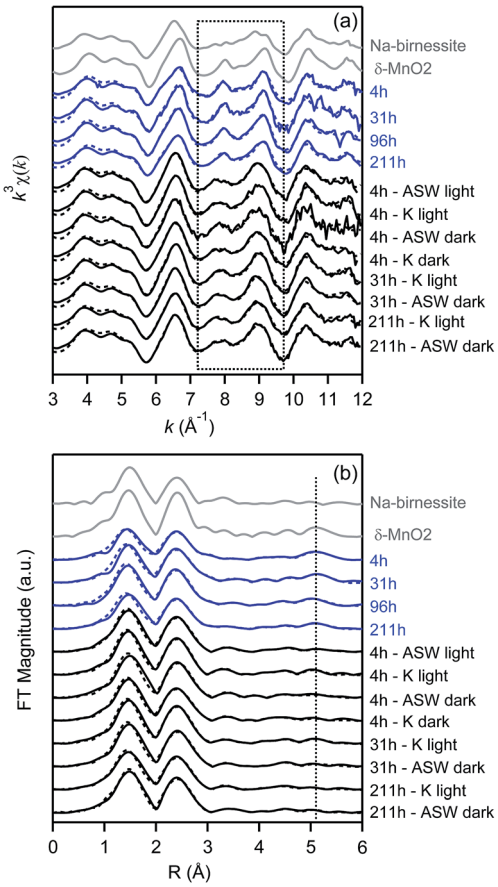

Fig. 2 Mn K-edge EXAFS data (a) and corresponding Fourier transforms (b) of reference compounds (grey lines) and bioMnOx before (blue lines) or after (black lines) reacting with Cr(III) (~200 h). Raw and fitted data are shown in solid and dashed lines, respectively. The box with the dotted line in (a) shows the "indicator" region of Mn EXAFS. The vertical dotted line in (b) labels the peak with major contributions from multiple scattering.

marine *Bacillus* sp. were a layered phyllomanganate with hexagonal sheet symmetry similar to that of δ-MnO_2 and transformed to pseudo-orthogonal sheet symmetry with a structure similar to that of triclinic birnessite. These results are in agreement with our findings and suggest that a gradual structural transformation of bioMnOx can be common in the nature, and might play an important role in the bioMnOx reactivity toward controlling metal speciation such as the oxidation of Cr(III).

Detailed structural fitting of the initial Mn oxides was consistent with the LCF results (Fig. 2, Table S2†). In particular, the initial colloidal Mn oxide phase (4 h) had a structure with a negligible out-of-plane bending of the octahedral layers ($\beta_a = 0$), a high number of corner-sharing Mn octahedra (CN = 3.2), and low fraction of occupied Mn octahedral sites ($f_{occ} = 0.64$). These values are in good agreement with the structural model for hexagonal birnessite[26] with a slightly lower f_{occ} value. Upon aging, the bioMnOx gradually transformed with structural parameters intermediate between hexagonal and triclinic birnessite. The out-of-plane bending angle β_a increased from zero to ~1.6, 6.9, and 7.4 for bioMnOx aged for 31, 96 and 211 hours, respectively, suggesting a gradual transformation of the bio-MnOx from hexagonal to triclinic symmetry over time and is consistent with the LCF results. Triclinic birnessite has pseudo-orthogonal symmetry and is characterized by a larger proportion (up to 1/3) of Mn(III) octahedra in the sheets compared to hexagonal birnessite.[42,43] The large angular non-linearity along the *a*-axis (β_a 12–17)[26,41] of triclinic birnessite is a result of lattice strain produced in the planar sheet buckling upon Mn(III)-rich row formation.[42]

Further and as expected, the dominant oxidation state of the bioMnOx was Mn(IV) with a minor component of Mn(III). Comparing the peak crest positions of bioMnOx with those of the reference compounds (vertical dotted lines) indicated that the bioMnOx all have a Mn valence state similar to that of δ-MnO_2, which has an average oxidation state of 3.9–4.0 (Fig. S1†). However, all bioMnOx spectra also showed peak broadening, with a small shoulder at ~6550 eV that is similar to that of the feitknechtite spectra, suggesting the presence of minor amounts of Mn(III) in the structure.

3.2. Cr(III) oxidation by structurally diverse biogenic Mn oxides under varying light and carbon conditions

The extent of Cr(VI) production was 2–10 times higher in the presence relative to the absence of bioMnOx, indicating that the

biogenic Mn oxides induced the oxidation of aqueous Cr(III) (Fig. 3). In detail, Cr(VI) production in the absence of Mn oxides averaged 0.55 μM (1.1% of added Cr(III)), which was substantially lower than that in the presence of bioMnOx (Fig. 3). Interestingly, control experiments conducted in the absence of Mn oxides and within the dark yielded Cr(VI) production close to zero, whereas those in the light within either cell-free filtrate, ASW, or K medium yielded small amounts of Cr(VI) production (0.5–1.5 μM). These values, although far less than those in the presence of bioMnOx, suggest a potential contribution of photoactive factors, such as reactive oxygen species (ROS) or organic radicals produced in the presence of light, in oxidizing Cr(III).

In the presence of bioMnOx, the rate and extent of Cr(III) oxidation varied as a function of Mn oxide structure (age), light, and organic carbon. In the absence of organic carbon (*i.e.*, in ASW) and/or under dark conditions, a significant difference between the Cr(III) oxidation capacity of differently aged MnOx was not observed (Fig. 4). However, in organic carbon-rich K medium in the presence of light, the Cr(III) oxidation capacity is highly dependent on the MnOx structure (age). In particular, more aged bioMnOx phases with a higher proportion of triclinic birnessite demonstrated lower reactivity. In fact, a linear correlation ($R^2 = 0.9897$; dotted line in Fig. 4) between Cr(III) oxidation capacity and MnOx age can be established. Note that all experiments were conducted with the same concentration of initial MnOx and Cr(III), therefore the differences in reactivity were likely due to variation in the intrinsic reactivity as the oxides aged from hexagonal to triclinic birnessite.

Despite many previous studies, the detailed reaction mechanism(s) of Cr(III) oxidation by Mn oxides remain unclear. It was showed that the Cr(III) oxidation ability of different manganese oxides can be related to, although not directly proportional to, the presence of structural Mn(III).[21] The availability of Mn(III) during the oxidation of Cr(III) by δ-MnO_2 was also shown to be an important controlling factor in that the presence of Mn(III) complexing ligand pyrophosphate during the reaction between

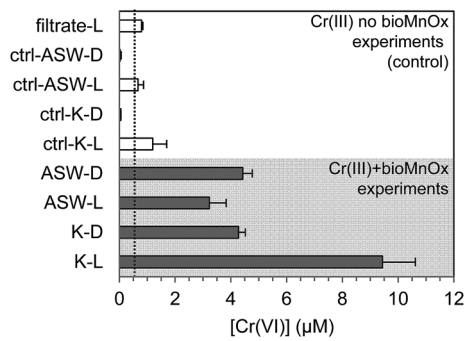

Fig. 3 Amount of Cr(VI) produced in the presence of 4 h aged bio-MnOx (filled bars) in artificial sea water (ASW) or K medium (K) at pH 7.2 under light (L) or dark (D) conditions. Also shown are the Cr(VI) production in control experiments (open bars), with the same amount of initial Cr(III) and no bioMnOx addition. They are conducted either in the cell-free filtrate, ASW, or K medium under light or dark conditions. The vertical dotted line is the averaged Cr(VI) production from all control experiments (0.55 μM). All values were measured when reactions reached near steady state (~200 h).

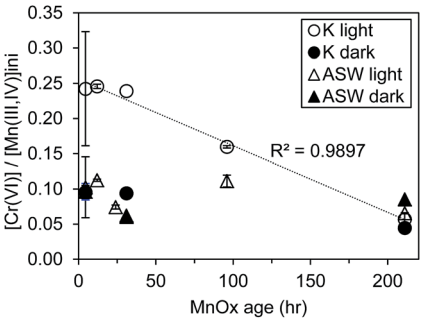

Fig. 4 Cr oxidation capacity as a function of bioMnOx age when reacted in K medium or ASW under light or dark conditions. The dotted line is a linear fitting of the K light data ($R^2 = 0.9897$). Reactions were conducted at pH 7.2.

Cr(III) and Mn oxide drastically reduced the Cr(III) oxidation rate.[13] The presence of Mn(II) has also been shown to enhance Cr(III) oxidation by synthetic manganese oxides (*e.g.*, hausmannite, Mn_3O_4)[21] or in systems containing Mn(II)-oxidizing microorganisms.[22,31–33] For these biotic systems, it is generally recognized that the oxidation of Cr(III) is mainly due to the formation of biogenic Mn oxides that are produced from the oxidation of Mn(II) by microorganisms.[23,34–36] However, in these studies, the presence of active cells complicates the investigations due to cell metabolism and/or the toxicity effect of Cr(VI), thus making it difficult to isolate the structural effect of the biologically formed Mn oxides. Here, we show also that light and organic carbon (Fig. 3–5, Table 1) complicate the direct assessment of the role of Mn oxide structure and composition in Cr(III) oxidation.

In particular, a substantial structural influence in the presence of carbon and light was observed for the initial hexagonal birnessite dominated Mn oxide phases (aged less than 50 hours). For 4 h old Mn oxides, the Cr(III) oxidation capacity was highest under combined light and carbon conditions, reaching ~0.20 at near steady state, whereas all other conditions (K dark, ASW light, or ASW dark) showed a similar Cr(III) oxidation capacity of ~0.07 (Fig. 5a). As minimal Cr(VI) was produced under K light conditions in the absence of Mn oxides, a mineral surface produced photoactive factor was likely at play. Mn oxides are versatile oxidants of a wide range of organic compounds such as hydroquinone, oxalic acid, and humic substances,[44–47] and the Mn oxide catalyzed oxidation of organics is known to produce reactive organic radicals.[45,48] Similarly, Learman *et al.*[27] implicated both mineral induced organic and oxygen radical formation in accelerated Mn(II) oxidation rates by colloidal hexagonal birnessite formed by this *Roseobacter* species. On the other hand, it is worth noting that Cr(III) can strongly complex with organic ligands such as citrate and EDTA, which can prevent the release of Cr(III) ions and subsequent oxidation by Mn oxides.[14,17] Although we observed enhanced Cr(VI) formation in the presence of organics, complexation of Cr(III) by media components (K medium is a rich medium containing peptone and yeast extract) could hypothetically limit the extent of Cr(VI) formation. At this stage, the exact photo-active factor or organic compound(s) in our

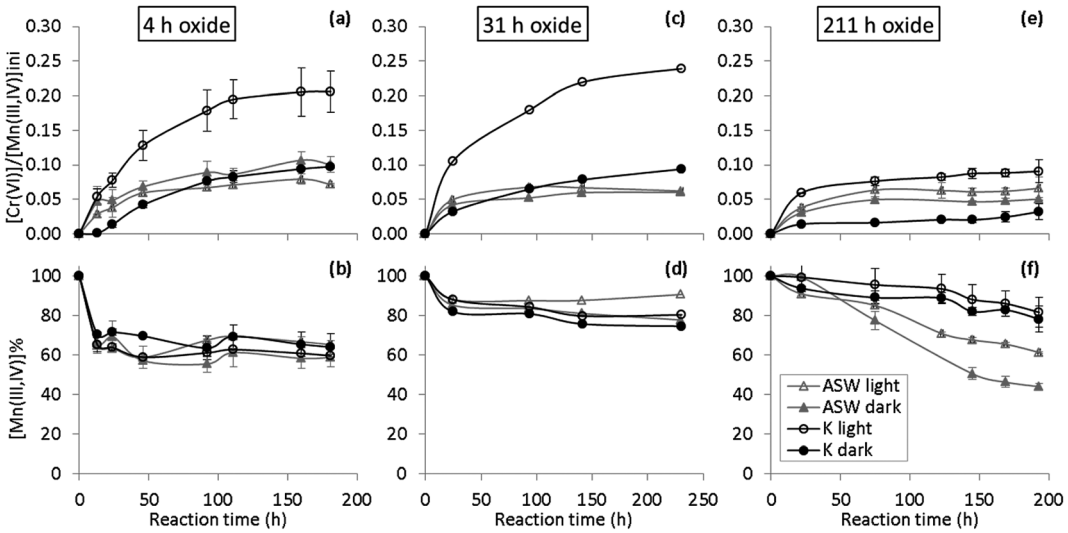

Fig. 5 Cr(III) oxidation capacity (a, c and e) and percent change of Mn(III,IV) oxide concentration (b, d and f) as a function of reaction time in the K medium or ASW under light or dark conditions. BioMnOx ages are 4 h (a and b), 31 h (d and e), and 211 h (e and f).

system is not clearly understood; partially due to the fact that the K medium is a rich organic matrix composed of a large diversity of organic nitrogen and carbon molecules. The identity of the reactive organic(s) and the reaction mechanisms is currently under investigation.

Interestingly, despite differences in Cr(VI) production by the initial hexagonal birnessite phase incubated under different conditions (Fig. 5a), a concomitant change in Mn oxide concentration was not observed (Fig. 5b). In detail, all experiments showed a similar sharp decrease in the Mn oxide concentration to ~65% of the initial concentration within 20 h, followed by a pseudo-steady state level that was maintained at ~60% throughout the remainder of the reaction (Fig. 5b). The 4 and 31 h aged bioMnOx showed similar Cr(VI) production and MnOx consumption trends (Fig. 5a–d). For the more triclinic bioMnOx (211 h aged), however, differences in Cr(VI) production and MnOx consumption varied based on the experimental conditions, with the carbon replete (K) light incubations still yielding the highest Cr(VI) production and the carbon-deplete (ASW) dark conditions showed the largest loss of Mn(III,IV) oxide.

The change in Mn oxide concentration likely involved a number of reactions, including decreased MnOx concentration through the redox reaction with Cr(III), photo-induced dissolution, and increased MnOx concentration *via* the abiotic oxidation of aqueous Mn(II) at the Mn oxide surface (production of

Table 1 Initial Cr(III) oxidation rate and total Cr(VI) production. All reactions conducted at pH 7.2 in either K medium or ASW under light or dark conditions

Reaction conditions	BioMnOx age (h)	n^a	Initial Cr(III) oxidation rate^b (μmol L^{-1} h^{-1})	Total Cr(VI) production^c (μM)
K Light	4.5	6	0.11–0.29	9.92 ± 3.11
	12	2	0.29–0.34	10.42 ± 0.36
	31	1	0.2	11.20
	96	3	0.15	6.15 ± 0.05
	211	2	0.09	1.97 ± 0.32
K Dark	4.5	3	0.02–0.03	3.53 ± 1.30
	31	1	0.06	4.36
	211	2	0.02	1.45 ± 0.08
ASW light	4.5	5	0.03–0.09	3.76 ± 0.75
	12	2	0.15	4.46 ± 0.05
	24	3	0.08–0.09	3.23 ± 0.12
	31	1	0.09	2.72
	96	3	0.13–0.16	4.56 ± 0.18
	211	2	0.06	2.29 ± 0.12
ASW dark	4.5	4	0.02–0.11	3.70 ± 1.24
	31	1	0.08	2.66
	211	2	0.05	3.04

^{a} Total number of experiments conducted under these conditions. ^{b} The rate of Cr(VI) production within initial 20 h. ^{c} The total amount of Cr(VI) produced in the reaction systems at near steady state (~200 h).

secondary Mn oxides).[49] Mn oxides,[50,51] especially highly reactive layered phyllomanganates,[52] can accelerate the oxidation of Mn(II) by O_2 through autocatalysis. Further, Learman *et al.*[27] reported that hexagonal birnessite- and light-mediated formation of carbon and oxygen radicals can lead to Mn(II) oxidation rates in excess of the competing photodissolution process.[27] Based on our Mn oxide and Cr(VI) concentration data, we postulate that this Mn (re)cycling is a likely mechanism responsible for the high Cr(III) oxidation capacity in the combined presence of light and organics in our system. In detail, during the initial 20 h, during which the Mn(III,IV) oxide concentration experienced a sharp decrease, the system is dominated by the redox reaction between primary bioMnOx and Cr(III), which produces Cr(VI) and presumably aqueous Mn(II). The produced Mn(II) can then be oxidized by carbon and/or oxygen radicals produced by reaction with the remaining bioMnOx to produce more secondary MnOx, which are also capable of oxidizing Cr(III). This process (cycling of Mn(II)) might explain the apparent higher Cr(III) oxidation capacity yet near steady state concentration of Mn oxide in the system. Alternatively, the carbon- and/or oxygen-radicals could directly oxidize Cr(III), yet, this would not explain the Mn oxide concentration trends (Fig. 5b) in combination with the persistence of hexagonal birnessite in the presence of light and carbon (discussed below).

3.3. Rates of Cr(III) oxidation

For all conditions, the rates of Cr(III) oxidation were fastest during the initial 20 h, slowly decreasing over time and plateauing between 50 and 150 hours (*e.g.* Fig. 5a, c and e). Initial Cr(III) oxidation rates, based on the amount of Cr(VI) production during the first 20 h, spanned an order of magnitude and were highly dependent upon the structure of the Mn oxide and the aqueous conditions (Table 1). For instance, the initial Cr(III) oxidation rate for the 4 h old bioMnOx was 0.11–0.29 μM h^{-1} under K light conditions, 0.02–0.03 μM h^{-1} under K dark conditions, and 0.02–0.11 μM h^{-1} under ASW conditions (light and dark).

Previous studies on the oxidation of Cr(III) by various manganese oxides showed varied reaction rates and capacity. Using Q-XAFS (quick X-ray absorption fine structure spectroscopy), Landrot *et al.*[11] showed that the oxidation of Cr(III) by three difference types of synthetic poorly crystalline layered manganese oxides (δ-MnO_2, random stacked birnessite, and acid birnessite) were fast within the first 30 min and ceased between 30 min and 1 h, which was explained as the sorption of Cr(VI) species on the Mn oxides. Dai *et al.*[17] also observed a fast increase of Cr(VI) levels in the presence of δ-MnO_2 within the initial ~50 min, followed by a very slow increase of Cr(VI) after 300 min, which was explained as the saturation of available surface adsorption sites.

Due to the difference in experimental conditions, it is difficult to directly compare the oxidation rates from our system with previous studies. Therefore we compared our results with Mn(II) oxidation rates by the same biooxides.[27] Consistent with Cr(III) oxidation, Learman *et al.*[27] found that more aged (more triclinic) bioMnOx phases yielded lower Mn(II) oxidation. Using 4 h aged colloidal hexagonal birnessite, they reported Mn(II) oxidation rates of 0.56–2.30 μM h^{-1} in the presence of organic carbon (K media) and light, 0.21–0.62 μM h^{-1} in K within the dark, and 0.08–0.27 μM h^{-1} in the absence of organic carbon (ASW). These values are substantially higher than the Cr(III) oxidation rates observed here, likely due to the difference in the nature of the reaction mechanism(s), *e.g.*, 3 electrons are needed to oxidize Cr(III) to Cr(VI), whereas only 1–2 electrons are needed to oxidize Mn(II) to Mn(III) or Mn(IV). However, both datasets follow a general trend that the combination of light and organic carbon yielded higher oxidation rates.

3.4. Mn oxide structural changes upon reaction with Cr(III)

The reacted bioMnOx samples appeared to be more triclinic as compared to the reference compound δ-MnO_2 (hexagonal birnessite structure), with a diminished oscillation at ~8 $Å^{-1}$ and broad feature at ~9 $Å^{-1}$ (Fig. 2). Detailed structural analysis revealed that all reacted samples transformed from the highly disordered hexagonal birnessite phase into more ordered phases similar to triclinic birnessite (Fig. 6 and Table S2†). For instance, the out-of-plane bending angles β_a are generally much higher than those of the unreacted samples. Interestingly, the 4 h aged bioMnOx, which possessed the highest oxidative capacity for Cr(III) in the presence of light and organic carbon (Fig. 4) yielded final Mn oxides with a lower β_a angle than the other three conditions (K dark, ASW light, and ASW dark) (Fig. 6). The 31 h aged bioMnOx also showed a lower β_a angle under K light conditions compared to the ASW dark conditions. These observations are consistent with our hypothesis that Mn(II) produced from the redox reaction between Cr(III) and the (primary) bioMnOx was recycled in the system and induced the (re)precipitation of (secondary) hexagonal birnessite. Such cycling was dominant under carbon-replete light conditions and the produced secondary Mn oxides restored the hexagonal Mn oxide reservoir in the system, thus resulting in an apparent steady state of the MnOx concentration (Fig. 5b and d) as well as lower β_a angles that correspond with the presence of more hexagonal phases (Fig. 6).

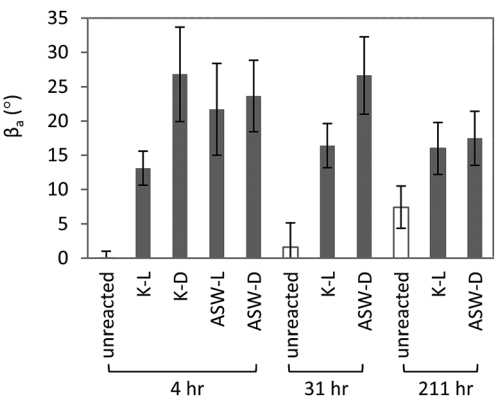

Fig. 6 Comparison of the out-of-plane bending along the *a*-axis (β_a angle) derived from EXAFS fitting of bioMnOx with different age and structural ripening before and after reaction with Cr(III) under different conditions.

In contrast, the 211 h aged bioMnOx had similar β_a angles after reaction under carbon-replete (K) light and -deplete (ASW) dark conditions. This is consistent with a similar lack in Cr(VI) production under these conditions (Fig. 4) and is likely due to the low reactivity of these more aged bioMnOx toward Cr(III) oxidation, Mn(II) oxidation, and thus production of secondary MnOx. The fact that both β_a angles were lower than those of the 4 and 31 h aged bioMnOx under dark and carbon-deplete (ASW) conditions is consistent with the overall low reactivity of 211 h aged bioMnOx.

3.5. Effect of pH and Mn oxide concentration

Cr(III) oxidation by abiotic Mn oxides has a strong pH dependence.[3,15] Here the oxidation of Cr(III) by 96 h aged bioMnOx reacted in the organic rich medium (K) under light conditions was substantially greater at pH 7.2 relative to 6.2 (Fig. 7b). At pH 7.2, Cr(III) oxidation had a fast initial reaction (within ~40 h) followed by a slow yet continuous process that reached steady state only after ~150 h, resulting in a final Cr oxidation capacity of ~0.16 (Fig. 7b). Correspondingly, the amount of bioMnOx in the reacting suspension quickly dropped to 87% within ~40 h, and slowly continued to ~80% after 160 h (Fig. 7a). The increase in Cr(VI) and decrease of bioMnOx levels was presumably dominated by the redox reaction between Cr(III) and bioMnOx, which involved the oxidation of Cr(III) to Cr(VI) and the reduction of Mn(III,IV) oxides to soluble Mn(II) species.

Interestingly, at pH 6.2 the Cr(III) oxidation capacity quickly increased to ~0.06 within ~10 h at a rate similar to that at pH 7.2, but then remained at this level throughout 160 h of reaction with no further significant production of Cr(VI) (Fig. 7b). The Mn oxide concentration decreased to ~85% during the first 10 h, and drastically dropped to only ~25% after 160 h reaction time (Fig. 7a). These observations are strikingly different from that at pH 7.2. At low pH, less Cr(VI) was produced but there was much greater loss of Mn(III,IV) oxides. In contrast, higher pH resulted in a much higher and continuous production of Cr(VI), accompanied by a near steady-state concentration of Mn oxides.

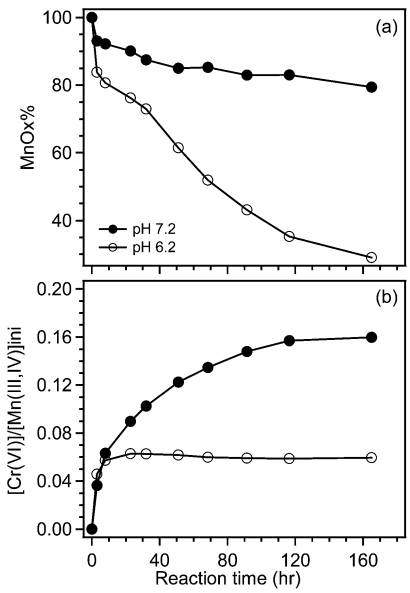

Fig. 7 Percent change of Mn(III,IV) oxide concentration (a) and Cr(III) oxidation capacity (b) as a function of reaction time at pH 6.2 and 7.2. Reaction conditions: 96 h aged bioMnOx, K medium, light condition.

Several studies have examined the effect of pH on Cr(III) oxidation by synthetic Mn oxides,[3,10,15] with an emphasis on acidic pH ranges. These studies observed that Mn oxides can strongly oxidize Cr(III) at lower pH ranges, and the pH effects were mainly contributed to two processes: (1) the adsorption of Cr(III) species on the surface of Mn oxides, which increases with increasing pH due to increased surface negative charge, and is favorable for more Cr(III) oxidation; and (2) the complexation of Cr(III) with hydroxyl groups and potential precipitation of Cr(III)-(oxyhydr)oxide phases, which is enhanced with increasing Cr(III) concentration and pH, and significantly decreases Cr(III) oxidation by Mn oxides. In our system, with the low Cr(III) concentration employed (50 μM), we do not expect the second mechanism to be significant. In fact, speciation calculations using the program Phreeqc[53] indicated that at both pH values our system was undersaturated with respect to solid Cr(III) (oxyhydr)oxide phases and the dominant Cr(III) species were $Cr(OH)_2^+$ and $CrOH^{2+}$.

The observations in our system appeared to be contradictory to previous studies in that a higher pH value yielded higher Cr(III) oxidation in our system. However, it is worth noting that all those studies used synthetic Mn oxides. In a few studies examining the oxidation of Cr(III) by biogenic manganese oxides formed *in situ*, pHs were controlled at near circumneutral values to maintain cell activity.[22,31–33] It is possible that (1) the biogenic Mn oxides formed under these conditions (including our system) might undergo proton-promoted dissolution under reduced pH conditions; and/or (2) that the activity of these biogenic Mn oxides toward Mn(II) oxidation and production of secondary Mn oxides is lower at low pH values. The detailed reaction mechanism(s) as well as the changed reactivity of bioMnOx under low pH conditions are under active investigation.

The Cr(III) oxidation capacity was also dependent on the initial bioMnOx concentration. Under both carbon-rich (K) light and -deplete (ASW) dark conditions, higher initial bioMnOx concentrations resulted in decreased Cr(III) oxidation capacity (Fig. S2†). Consistent with our previous observations, Cr(VI) oxidation efficiencies were higher under K light than under ASW dark conditions. All values were obtained after the reaction proceeded for ~150 h, representing near steady state values. Given all the same reaction conditions, one might expect the Cr(III) oxidation capacity to maintain a constant value regardless of the Mn oxide concentration. The fact that it decreased with increasing Mn oxide concentration was likely due to aggregation effects. Mineral particle aggregation and/or collision at high concentrations can decrease the effective surface area and result in lower degrees of contact with Cr(III).

4. Environmental implications

To the best of our knowledge, this is the first study exploring the effect of structural evolution of biogenic Mn oxides on the

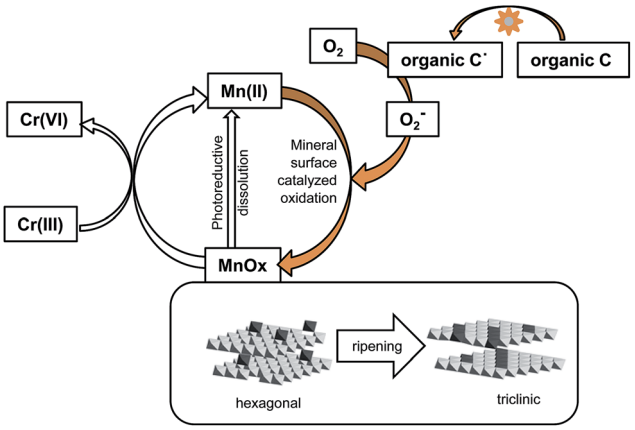

Fig. 8 Schematic of the possible reaction mechanism. Orange arrows represent reactions that occur only in the combined presence of organics and light.

oxidation of Cr(III) under various geochemical conditions. Here, as schematically illustrated in Fig. 8, we show that Cr(III) oxidation occurs to a much greater extent *via* reaction with hexagonal birnessite in the presence of both light and organic carbon. The production of photo-active factors, presumably organic- and/or oxygen-radicals, likely induces the (re)cycling of Mn in the system yielding substantially higher Cr(III) oxidation extent and rates. These surface mediated reactions in the presence of light and organics are apparently great enough to offset photo-dissolution of Mn oxides and allow for sustained oxidative capacity. The regeneration of reactive hexagonal birnessite under these conditions suggests that the speciation and fate of Cr in the natural environment might be dictated by even just a small amount of Mn oxides. Given the ubiquitous presence of Mn oxides in nature and that nanoparticulate hexagonal birnessite is the dominant Mn oxide formed by both terrestrial and marine microorganisms, this cycling scenario might play a substantial role in controlling the speciation of numerous redox sensitive elements, such as other metals and organic compounds.

Acknowledgements

The authors acknowledge funding support by Georgia Institute of Technology to YT and NSF grant CBET-1336496 to CMH. Portions of this research were conducted at the Stanford Synchrotron Radiation Lightsource (SSRL) and the National Synchrotron Light Source (NSLS). SSRL is a Directorate of SLAC National Accelerator Laboratory and an Office of Science User Facility operated for the U.S. Department of Energy Office of Science by Stanford University. NSLS is supported by the US Department of Energy, Office of Science, Office of Basic Energy Sciences, under Contract no. DE-AC02-98CH10886. Comments from two anonymous reviewers helped improving the manuscript.

References

1 C. D. Palmer and P. R. Wittbrodt, *Environ. Health Perspect.*, 1991, **92**, 25–40.
2 R. P. Beliles, in *Toxicity of Heavy Metals in the Environment (Part II)*, ed. F. W. Oehme and M. Dekker, New York, 1979.
3 S. E. Fendorf and R. J. Zasoski, *Environ. Sci. Technol.*, 1992, **26**, 79–85.
4 Y. Z. Tang and S. T. Martin, *Geochim. Cosmochim. Acta*, 2011, **75**, 4951–4962.
5 L. E. Eary and D. Rai, *Environ. Sci. Technol.*, 1987, **21**, 1187–1193.
6 Y. Z. Tang, F. M. Michel, L. H. Zhang, R. Harrington, J. B. Parise and R. J. Reeder, *Chem. Mater.*, 2010, **22**, 3589–3598.
7 B. M. Sass and D. Rai, *Inorg. Chem.*, 1987, **26**, 2228–2232.
8 S. E. Fendorf, *Geoderma*, 1995, **67**, 55–71.
9 R. Bartlett and B. James, *J. Environ. Qual.*, 1979, **8**, 31–35.
10 S. E. Fendorf, M. Fendorf, D. L. Sparks and R. Gronsky, *J. Colloid Interface Sci.*, 1992, **153**, 37–54.
11 G. Landrot, M. Ginder-Vogel, K. Livi, J. P. Fitts and D. L. Sparks, *Environ. Sci. Technol.*, 2012, **46**, 11594–11600.
12 G. Landrot, M. Ginder-Vogel, K. Livi, J. P. Fitts and D. L. Sparks, *Environ. Sci. Technol.*, 2012, **46**, 11601–11609.
13 P. S. Nico and R. J. Zasoski, *Environ. Sci. Technol.*, 2000, **34**, 3363–3367.
14 Y. M. Tzou, R. H. Loeppert and M. K. Wang, *Soil Sci.*, 2002, **167**, 729–738.
15 X. H. Feng, L. M. Zhai, W. F. Tan, W. Zhao, F. Liu and J. Z. He, *J. Colloid Interface Sci.*, 2006, **298**, 258–266.
16 C. Oze, D. K. Bird and S. Fendorf, *Proc. Natl. Acad. Sci. U. S. A.*, 2007, **104**, 6544–6549.
17 R. A. Dai, J. Liu, C. Y. Yu, R. Sun, Y. Q. Lan and J. D. Mao, *Chemosphere*, 2009, **76**, 536–541.
18 R. M. Weaver, M. F. Hochella and E. S. Ilton, *Geochim. Cosmochim. Acta*, 2002, **66**, 4119–4132.
19 G. Landrot, M. Ginder-Vogel and D. L. Sparks, *Environ. Sci. Technol.*, 2010, **44**, 143–149.
20 J. G. Kim, J. B. Dixon, C. C. Chusuei and Y. J. Deng, *Soil Sci. Soc. Am. J.*, 2002, **66**, 306–315.
21 R. M. Weaver and M. F. Hochella, *Am. Mineral.*, 2003, **88**, 2016–2027.
22 J. Z. He, Y. T. Meng, Y. M. Zheng and L. M. Zhang, *J. Soils Sediments*, 2010, **10**, 767–773.
23 B. M. Tebo, J. R. Bargar, B. G. Clement, G. J. Dick, K. J. Murray, D. Parker, R. Verity and S. M. Webb, *Annu. Rev. Earth Planet. Sci.*, 2004, **32**, 287–328.
24 J. R. Bargar, B. M. Tebo, U. Bergmann, S. M. Webb, P. Glatzel, V. Q. Chiu and M. Villalobos, *Am. Mineral.*, 2005, **90**, 143–154.
25 M. Villalobos, B. Toner, J. Bargar and G. Sposito, *Geochim. Cosmochim. Acta*, 2003, **67**, 2649–2662.
26 S. M. Webb, B. M. Tebo and J. R. Bargat, *Am. Mineral.*, 2005, **90**, 1342–1357.
27 D. R. Learman, S. D. Wankel, S. M. Webb, N. Martinez, A. S. Madden and C. M. Hansel, *Geochim. Cosmochim. Acta*, 2011, **75**, 6048–6063.
28 X. H. Feng, M. Q. Zhu, M. Ginder-Vogel, C. Y. Ni, S. J. Parikh and D. L. Sparks, *Geochim. Cosmochim. Acta*, 2010, **74**, 3232–3245.
29 E. J. Elzinga, *Environ. Sci. Technol.*, 2011, **45**, 6366–6372.

30 B. M. Tebo, H. A. Johnson, J. K. McCarthy and A. S. Templeton, *Trends Microbiol.*, 2005, **13**, 421–428.
31 Y. X. Wu, B. L. Deng, H. F. Xu and H. Kornishi, *Geomicrobiol. J.*, 2005, **22**, 161–170.
32 K. J. Murray and B. M. Tebo, *Environ. Sci. Technol.*, 2007, **41**, 528–533.
33 K. J. Murray, M. L. Mozafarzadeh and B. M. Tebo, *Geomicrobiol. J.*, 2005, **22**, 151–159.
34 C. M. Hansel, C. A. Zeiner, C. M. Santelli and S. M. Webb, *Proc. Natl. Acad. Sci. U. S. A.*, 2012, **109**, 12621–12625.
35 Y. Z. Tang, C. A. Zeiner, C. M. Santalli and C. M. Hansel, *Environ. Microbiol.*, 2013, **15**, 1063–1077.
36 D. R. Learman, B. M. Voelker, A. I. Vazquez-Rodriguez and C. M. Hansel, *Nat. Geosci.*, 2011, **4**, 95–98.
37 C. M. Hansel and C. A. Francis, *Appl. Environ. Microbiol.*, 2006, **72**, 3543–3549.
38 W. E. Krumbein and H. J. Altmann, *Helgolander Wissenschaftliche Meeresuntersuchungen*, 1973, **25**, 347–356.
39 S. M. Webb, *Phys. Scr.*, 2005, **T115**, 1011–1014.
40 B. Ravel and M. Newville, *J. Synchrotron Radiat.*, 2005, **12**, 537–541.
41 T. Ressler, S. L. Brock, J. Wong and S. L. Suib, *J. Phys. Chem. B*, 1999, **103**, 6407–6420.
42 B. Lanson, V. A. Drits, Q. Feng and A. Manceau, *Am. Mineral.*, 2002, **87**, 1662–1671.
43 E. Silvester, A. Manceau and V. A. Drits, *Am. Mineral.*, 1997, **82**, 962–978.
44 A. T. Stone and J. J. Morgan, *Environ. Sci. Technol.*, 1984, **18**, 450–456.
45 A. T. Stone and J. J. Morgan, *Environ. Sci. Technol.*, 1984, **18**, 617–624.
46 Y. Wang and A. T. Stone, *Geochim. Cosmochim. Acta*, 2006, **70**, 4477–4490.
47 W. G. Sunda and D. J. Kieber, *Nature*, 1994, **367**, 62–64.
48 Y. Ono, T. Matsumura and S. Fukuzumi, *J. Chem. Soc., Perkin Trans. 2*, 1977, 1421–1424, DOI: 10.1039/p29770001421.
49 W. G. Sunda and S. A. Huntsman, *Deep Sea Res. Oceanogr. Res. Paper.*, 1988, **35**, 1297–1317.
50 J. J. Morgan, Manganese and Its Role in Biological Processes, in *Metal Ions in Biological Systems*, ed. A. Sigel and H. Sigel, 2000, vol. 37, pp. 1–34.
51 J. J. Morgan, *Geochim. Cosmochim. Acta*, 2005, **69**, 35–48.
52 R. W. Coughlin and I. Matsui, *J. Catal.*, 1976, **41**, 108–123.
53 D. L. Parkhurst and C. A. J. Appelo, *User's guide to PHREEQC (Version 2) – a computer program for speciation, batch-reaction, one-dimensional transport, and inverse geochemical calculations*, U. S. Geol. Surv. Water Res. Inv., Rept. 99–4259, 1999.

